

Synthesis and Photoluminescence Properties of Tunable Green-Orange Cerium-Doped Terbium-Lutetium Aluminum Garnet

Jun Wang^{1,2}, Tao Han^{1,*}, Tianchun Lang^{1,2}, Mingjing Tu¹, Lingling Peng¹

¹ Research Institute for New Materials Technology, Chongqing University of Arts and Sciences, Chongqing 402160, People's Republic of China

² School of Material Science and Engineering, Chongqing University of Technology, Chongqing 400054, People's Republic of China

*E-mail: danbaiht@126.com

Received: 24 November 2014 / Accepted: 27 December 2014 / Published: 19 January 2015

Cerium-doped terbium-lutetium aluminum garnet ((Tb_xLu_{1-x})_{2.9}Al₅O₁₂: 0.1Ce) were synthesized by solid state reaction method. The crystalline phase, morphology and photoluminescence properties were characterized by using X-ray diffraction (XRD), photoluminescence (PL) spectra, scanning electron microscope (SEM) and color coordinates analysis, respectively. The results show that with the increasing amount of x (Tb³⁺), Lu₃Al₅O₁₂ (LuAG) phase changes gradually to Tb₃Al₅O₁₂ (TAG) phase with single-crystalline characteristic, and the average particle size of the powders increases. Because of the result of a decrease of the difference between the energy centroids of the 5d and 4f configurations and an increase of the effective ligand field on the Ce-5d shell, the emission spectrum of the samples has a red-shift of 37 nm and shifts toward the saturated colors, but the emission intensity decreases. The findings indicate that it could make the garnet phosphors green to orange tunable for the applications of white LED using the mutual doping effects of Lu³⁺ and Tb³⁺ in garnet structure.

Keywords: terbium-lutetium; cerium-doped garnet; morphology; photoluminescence; red-shift

1. INTRODUCTION

So far, white light-emitting diodes (LEDs) have been widely applied in many fields due to their many advantages, such as high efficiency, energy saving, long lifetime, reliability and safety [1-3]. For example, the LED has a potential application in the electrochemical, especially in the electrochemical deposition [4]. There are two main methods to realize the white LED device, one is wavelength conversion method, with blue LED chip excitation yellow phosphors(or red, green phosphors); two is color mixing, i.e. with near UV LED chip excitation red, green, blue three primary colors phosphors to

realize white light. Thus, the phosphor, composed of matrix and activator, is the key technology and one of the raw materials of WLED.

Up to now, the garnet family [5], including yttrium aluminum garnet ($\text{Y}_3\text{Al}_5\text{O}_{12}$, YAG) [6-8], lutetium aluminum garnet ($\text{Lu}_3\text{Al}_5\text{O}_{12}$, LuAG) [9-11], terbium aluminum garnet ($\text{Tb}_3\text{Al}_5\text{O}_{12}$, TAG) [12-14] etc, is commonly used for LED. However, the phosphors have some limitations, such as high color temperature, low color rendering index, become barriers to the application of white LED on some fields which have high demands of light source.

Many researchers control the color to improve the luminescence properties by means of codoping in garnet structure, for example, Kong et al. [15] observed that the Gd^{3+} makes the emission of $(\text{Y}_{0.96-x}\text{Gd}_x)_3\text{Al}_5\text{O}_{12}:\text{Ce}_{0.12}$ move to red spectral region, but the smaller one of Lu^{3+} makes it blue. Shao et al. [16] illuminated that with increasing the content of Lu^{3+} , the luminescence of $(\text{Y}, \text{Lu})_3\text{Al}_5\text{O}_{12}:\text{Ce}$ phosphors shows a pronounced blue-shift; Dotsenko et al. [17] demonstrated that the substitution of Tb^{3+} for Y^{3+} in the garnet structure results in broadening the emission band and shifting its maximum towards the longer wavelengths. Setlur et al. [18] demonstrated that significant DD migration can change the mechanism for DA energy transfer from a dipole-dipole to an exchange mechanism using Tb^{3+} donors and Ce^{3+} acceptors in $(\text{Lu}, \text{Tb})_3\text{Al}_5\text{O}_{12}:\text{Ce}^{3+}$ phosphors, however, they did not study on the morphology and particle size of the samples, which have an important influence on luminescence properties. Therefore, to further investigate the properties of $(\text{Tb}, \text{Lu})_3\text{Al}_5\text{O}_{12}:\text{Ce}^{3+}$, such as the morphology, in the present work, we prepared green to orange tunable cerium-doped terbium-lutetium aluminum garnet $(\text{Tb}_x\text{Lu}_{1-x})_{2.9}\text{Al}_5\text{O}_{12}:0.1\text{Ce}$ by solid state reaction method, and their luminescence properties, morphology, particle size were systematically investigated.

2. EXPERIMENTAL

2.1. Sample preparation

All the samples were synthesized by high-temperature solid-state reaction under reducing atmosphere. According to the stoichiometric ratios of $(\text{Tb}_x\text{Lu}_{1-x})_{2.9}\text{Al}_5\text{O}_{12}:0.1\text{Ce}$ ($x=0, 0.2, 0.5, 0.8$ and 1.0), the starting materials of Lu_2O_3 (99.99%), Tb_4O_7 (99.99%), CeO_2 (99.99%), Al_2O_3 (AR) were mixed with adding BaF_2 (AR) as flux (5% (mass fraction)). The mixtures added with appropriate alcohol were milled thoroughly for 10 h, and then dried in a drying oven at $80\text{ }^\circ\text{C}$ for 1 h as precursor. Finally, the precursor was sintered at $1600\text{ }^\circ\text{C}$ for 10 h, and then reduced at $1500\text{ }^\circ\text{C}$ for 2 h in an atmosphere with H_2 . Finally, the samples were obtained after milled.

2.2. Characterization

Crystalline phase of samples was analyzed by powder X-ray diffraction (XRD) on an X-ray diffractometer (TD-3500, Dandong, China) using $\text{Cu K}\alpha 1$ radiation at 30 KV and 20 mA. The XRD data were collected by a scanning mode in the 2θ range from 10° to 70° with a scanning step of 0.02° and a scanning rate of $2.0^\circ\text{ min}^{-1}$. Surface morphology and particle size were obtained by a scanning

electron microscope (SEM, Quanta 250, FEI, USA) with accelerating voltage of 10 kV. Photoluminescence (PL) properties were recorded with a fluorescence spectrophotometer (F-7000, Hitachi, Japan) with a 150 W xenon lamp at room temperature. Commission Internationale de l'Eclairage (CIE) color coordinates were characterized using a HSP3000 high accuracy LED photo-color and electron test system (Hangzhou Hongpu Optoelectronics Technology Co. Ltd., China), and evaluated under a current of 350 mA.

3. RESULTS AND DISCUSSION

3.1. Structure and morphology

In order to inform the crystalline structure of the obtained phases, we made a comparison sample uniformly mixed by the same molar ratio of LuAG: Ce_{0.1} and TAG: Ce_{0.1}. Fig.1 shows the XRD patterns of (Tb_{0.5}Lu_{0.5})_{2.9}Al₅O₁₂: 0.1Ce and the comparison sample. It can be seen that the comparison sample displays two characteristic peaks which are assigned to LuAG (JCPDS 18-0761) and TAG (JCPDS 17-0735), respectively, but the diffraction peaks of (Tb_{0.5}Lu_{0.5})_{2.9}Al₅O₁₂: 0.1Ce are sharper and show single-crystalline characteristic, and its position is obviously different from comparison sample, indicating that the mutual dopants of Tb³⁺ and Lu³⁺ could entirely dissolve in the single garnet structure of the obtained samples.

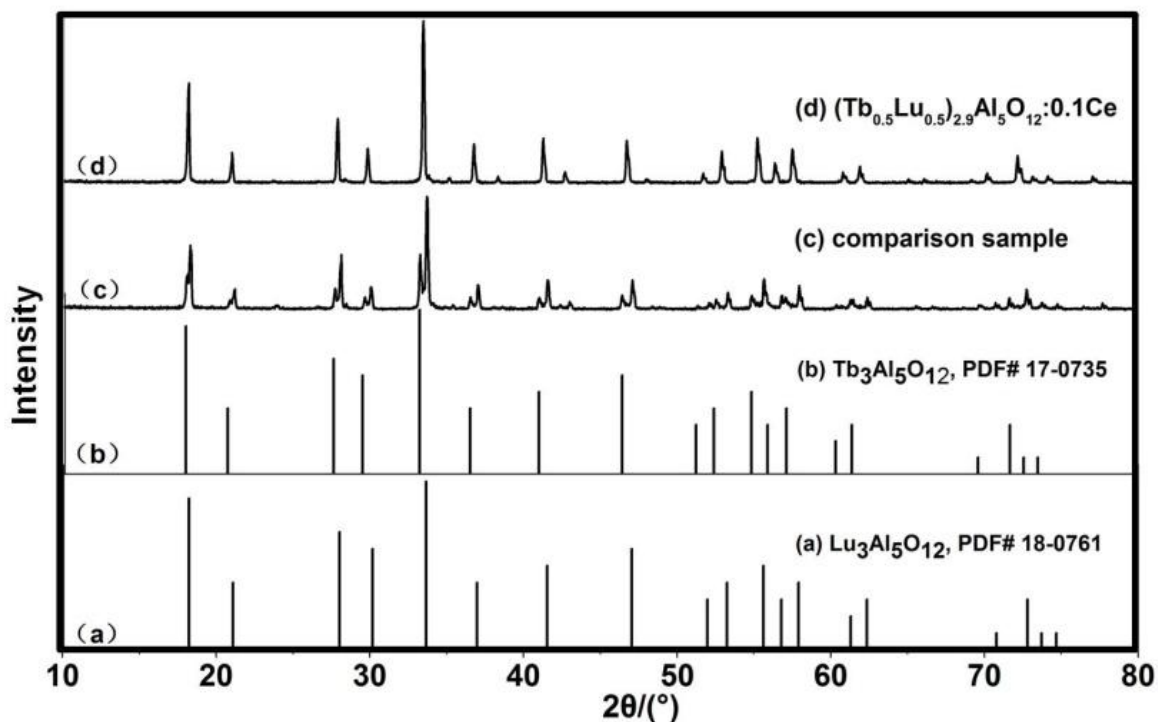


Figure 1. XRD patterns of (Tb_{0.5}Lu_{0.5})_{2.9}Al₅O₁₂: 0.1Ce and the comparison sample.

Fig.2 shows the XRD patterns of $(\text{Tb}_x\text{Lu}_{1-x})_{2.9}\text{Al}_5\text{O}_{12}: 0.1\text{Ce}$ ($x=0, 0.2, 0.5, 0.8,$ and 1.0). When x ranges from 0 to 1.0, the positions of diffraction peak shift to the small angle (see the inset). The diffraction angle can be calculated by the Bragg Equation,

$$2d \sin \theta = n\lambda \quad (1)$$

Where d is the interplanar distance, λ is the wavelength of X-ray and θ is the diffraction angle. According to Bragg equation, the diffraction angle decreases depending on the increase of the interplanar distance. As discussed above, Tb^{3+} ion with larger radii ($r(\text{Tb}^{3+}) = 0.0923 \text{ nm}$) substitutes Lu^{3+} ion ($r(\text{Lu}^{3+}) = 0.0848 \text{ nm}$) in the garnet host lattice, contributed to crystal cell expansion and the increase of interplanar distance. As shown in Fig. 2, with the substitution of Lu^{3+} ion sites by Tb^{3+} ion in garnet structure, the samples with different concentration of Tb^{3+} doped into LuAG: Ce are still in pure phases and when Tb^{3+} substitutes Lu^{3+} in the garnet host lattice, the phase is also a cubic structure.

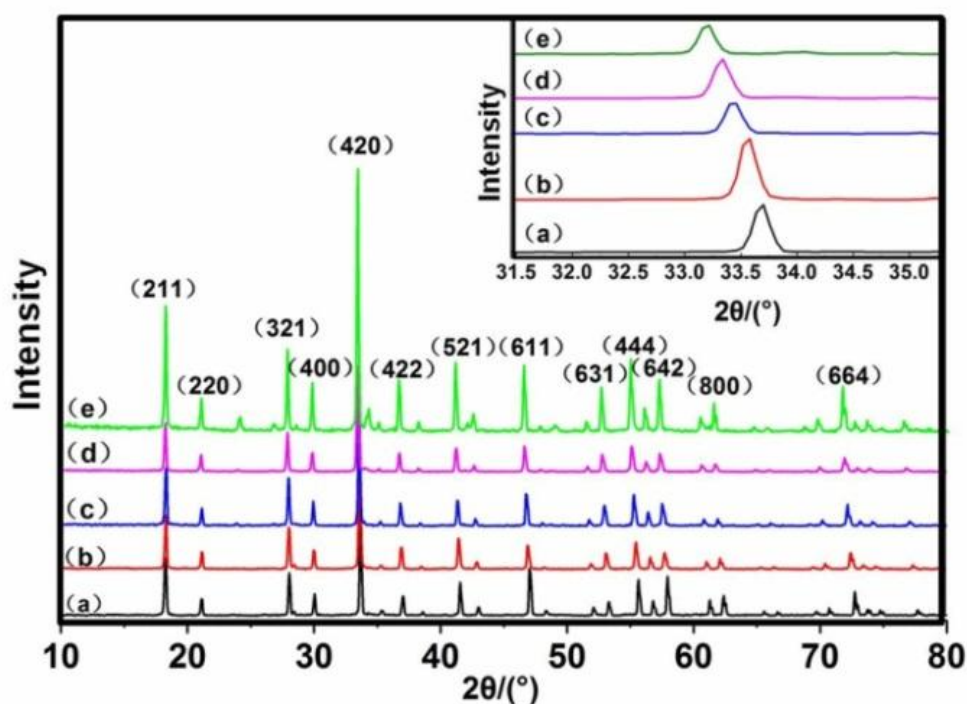


Figure 2. XRD patterns of $(\text{Tb}_x\text{Lu}_{1-x})_{2.9}\text{Al}_5\text{O}_{12}: 0.1\text{Ce}$ phosphors. a~e: $x=0, 0.2, 0.5, 0.8,$ and 1.0 .

The SEM morphologies of $(\text{Tb}_x\text{Lu}_{1-x})_{2.9}\text{Al}_5\text{O}_{12}: 0.1\text{Ce}$ are shown in Fig. 3. The obtained samples are nearly spherical shape, and agglomerate with the increase of x (Tb^{3+}). As $x=0$, the particle size of the sample is about $2.0\text{-}4.0 \mu\text{m}$ (Fig.3a); as $x=1$, the particle size of the sample increase to $6.0\text{-}8.0 \mu\text{m}$ (Fig.3e). Plainly, with the increase of the amount of Tb^{3+} ion, the particle size has an obvious growing up. This is attributed to crystal cell expansion, where the larger Tb^{3+} ion gradually substitutes the smaller Lu^{3+} ion.

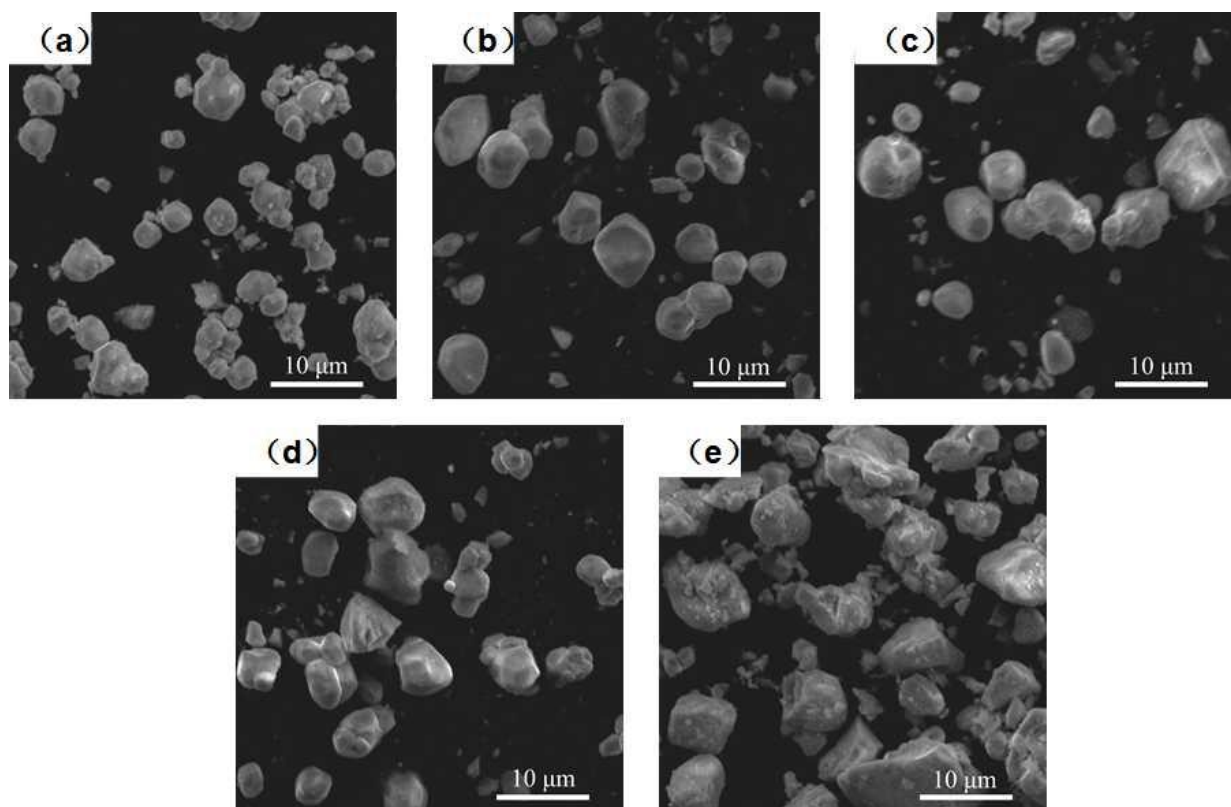


Figure 3. SEM morphologies of $(\text{Tb}_x\text{Lu}_{1-x})_{2.9}\text{Al}_5\text{O}_{12}: 0.1\text{Ce}$ phosphors. a~e: $x=0, 0.2, 0.5, 0.8,$ and 1.0 .

The photoluminescence excitation spectra of $(\text{Tb}_x\text{Lu}_{1-x})_{2.9}\text{Al}_5\text{O}_{12}: 0.1\text{Ce}^{3+}$ are shown in Fig. 4. As shown in Fig.4, three distinct excitation bands appear centered at around 340 nm, 375 nm, and 450 nm, respectively. Of these, the two stronger bands with peak at 340 and 450 nm originate from a transition from 4f-5d of Ce^{3+} ion, but the weaker band peak at 375 nm coincides with the f-f transition of Tb^{3+} ion. This is in agreement with the report in the literature [19]. Moreover, with the increase of the amount of Tb^{3+} ion, the excitation peak around 450 nm has a red shift, meanwhile, the peak around 375 nm has a blue shift. The fact that when Tb^{3+} substitute Lu^{3+} , the LuAG: Ce has two 4f→5d absorptions, the first 4f→5d absorption resulted to be a red shift, in opposition to the blue shift of the second absorption. Furthermore, the blue shift of the second 4f→5d transition is mostly due to ligand field effects, which result mainly from an important rising of the 2-5d level among the 5d manifold, most of it due to the first-shell distortion[20]. Except the two shifts, the excitation peak around 375 nm has no shift, but the relative intensity increases, and when $x=0.8$, the intensity is the maximum. This can be explained by that with the increase of the amount of Tb^{3+} , Tb^{3+} ion becomes to the luminescent center, then the intensity increases. And when the amount of Tb^{3+} exceeds a certain threshold value, the intensity decreases, i.e. concentration quenching. Although the peak has a red or blue shift, however, the relative intensity of excitation peaks decreases with the increasing amount of Tb^{3+} in the garnet structure.

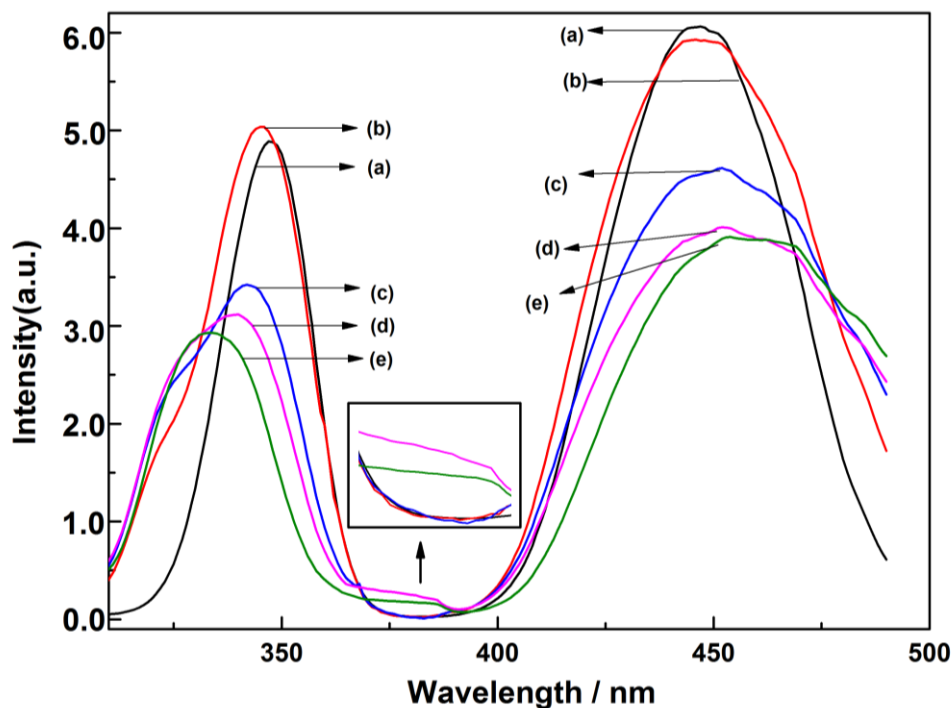


Figure 4. Excitation spectra of $(Tb_xLu_{1-x})_{2.9}Al_5O_{12}: 0.1Ce$ phosphors. a~e: $x=0, 0.2, 0.5, 0.8,$ and 1.0 .

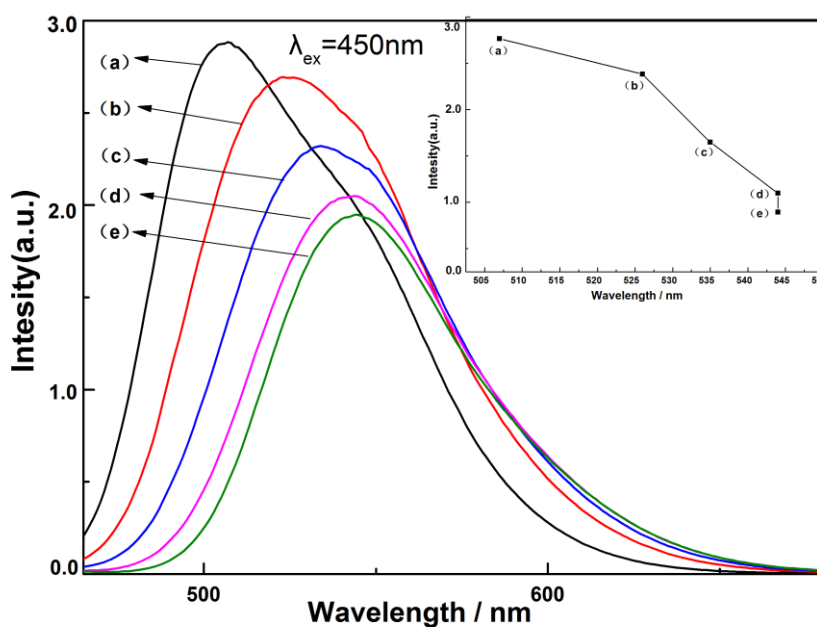


Figure 5. Emission spectra of $(Tb_xLu_{1-x})_{2.9}Al_5O_{12}: 0.1Ce$ phosphors. a~e: $x=0, 0.2, 0.5, 0.8,$ and 1.0 . Inset is the relationship between $x(Tb^{3+})$ and PL intensity

The emission spectra of $(Tb_xLu_{1-x})_{2.9}Al_5O_{12}: 0.1Ce$ excited by 450 nm light are presented in Fig. 5. Usually, the Ce^{3+} emission is in near-UV region, but the dominant wavelengths of LuAG: Ce and TAG: Ce are observed in the visible region, which correspond to the 4f-5d transition of Ce^{3+} ion.

When Tb^{3+} replaces Lu^{3+} site completely, the emission band shifts toward a longer wavelength by about 37 nm (507 nm to 544 nm) and the color of sample turns green to orange. In addition, the emission intensity of the sample excited by 450 nm light decreases with the increase of the amount of Tb^{3+} .

The red shift is the result of a decrease of the difference between the energy centroids of the 5d and 4f configurations and an increase of the effective ligand field on the Ce-5d shell associated with electronic effects of Tb^{3+} substituting for Lu^{3+} . It is known that the larger ionic radii of Gd^{3+} and of La^{3+} with respect to Y^{3+} make the lattice constant increase [21,22], and Tb^{3+} substituting Lu^{3+} also has the similar effect. This effect, together with the lattice expansion, the dopings create local compressions around Ce^{3+} ion, which increase the ligand field acting on the Ce-5d shell, and consequently, lower the first 5d energy level.

Moreover, according to crystal field theory, the site symmetry, ligand charge, bond length and covalence have important influence on the crystal field strength [23]. Crystal field splitting (Dq) can be calculated by the following Equation [24].

$$Dq = \frac{1}{6} Z e^2 \frac{r^4}{R^5} \quad (2)$$

Where Dq is a measure of the energy level separation, Z is the charge or valence of the anion, e is the charge of an electron, r is the radius of the wave function, and R is the bond length. When Lu^{3+} site was substituted by a larger Tb^{3+} ion, the distance between Ce^{3+} and O^{2-} became shorter [25]. Since crystal field splitting is proportional to $1/R^5$, the short Ce-O distance increases the crystal field splitting, also lower the 5d energy level with respect to the 4f ground state. Furthermore, caused by the increase of crystal field splitting of Ce^{3+} , the nonradiative transition increases. This is unfavourable for the luminescence of Ce^{3+} , consequently, the intensity decreases.

Fig.6 shows the energy level diagrams of Ce^{3+} . As shown in Fig. 6, the Ce^{3+} has a $4f^1$ configuration and its excited configuration is $4f^05d^1$ state. The 5d electron of the excited $4f^05d^1$ configuration forms a 2D term split into ${}^2D_{3/2}$ and ${}^2D_{5/2}$ states, and the 4f electron of the ground $4f^1$ configuration forms ${}^2F_{7/2}$ and ${}^2F_{5/2}$ states by spin-orbit coupling. When the sample is illuminated by blue light, it absorbs strongly blue light, and the yellow light is emitted by transition from the lowest 5d band to the ${}^2F_{7/2}$ and ${}^2F_{5/2}$ states of the Ce^{3+} ion [23]. Since 5d level is located beyond the orbit of 5s5p, and is not shield by the electronic shell. No doubt that when Tb^{3+} ion substitutes the Lu^{3+} ion, the 5d level suffers a nephelauxetic effect, then the 5d energy level lowers, and the energy difference between the energy centroids of the $5d^1$ and $4f^1$ configurations decreases. The energy difference can be expressed as follows Equation [26].

$$\Delta E(\text{eV}) = hv = 1.24/\lambda(\mu\text{m}) \quad (3)$$

Where ΔE is the energy difference between the energy centroids of the $5d^1$ and $4f^1$ configurations, λ is the wavelength of an electron. When the energy level difference decreases, the wavelength increases, i.e. red shift occurs.

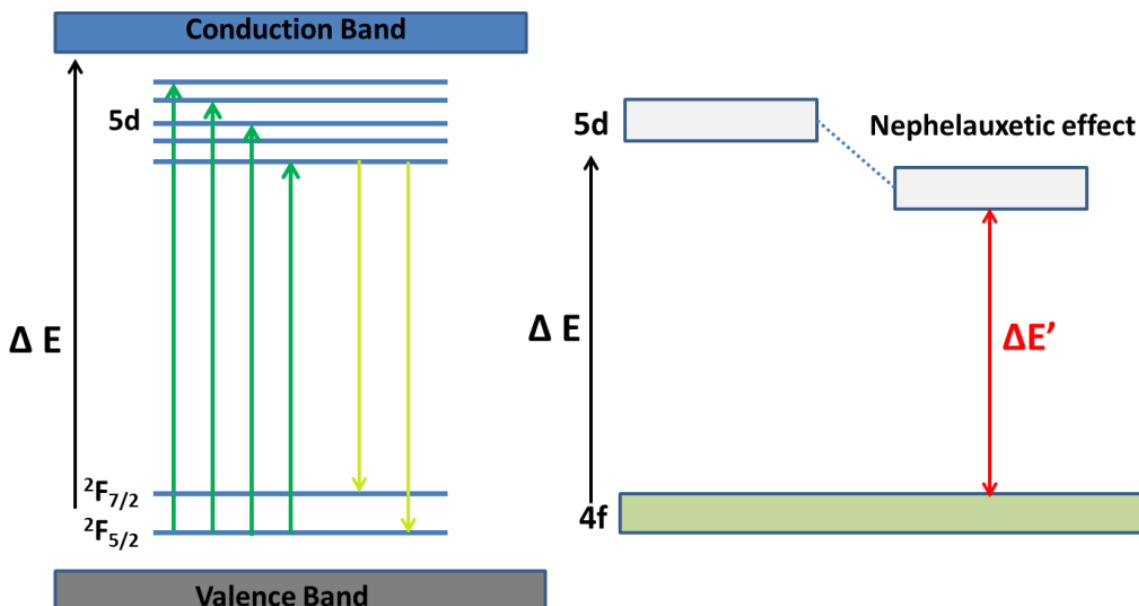


Figure 6. Energy level diagrams of Ce^{3+}

The Gaussian curve fittings of $(Tb_xLu_{1-x})_{2.9}Al_5O_{12}: 0.1Ce(x=0,1.0)$ are shown in Fig. 7. According to the Gaussian curve fittings, we can see that the emission bands are composed of two broad bands, assigned to the ${}^2F_{5/2}$ and ${}^2F_{7/2}$ transition of Ce^{3+} . With the increasing amount of Tb^{3+} , the two bands show obvious red-shift, one shifts by 1448 cm^{-1} (from 20000 cm^{-1} to 18552 cm^{-1}) and the other shifts by 1371 cm^{-1} (from 18762 cm^{-1} to 17391 cm^{-1}). This is almost in agreement with the wavelength of the red shift.

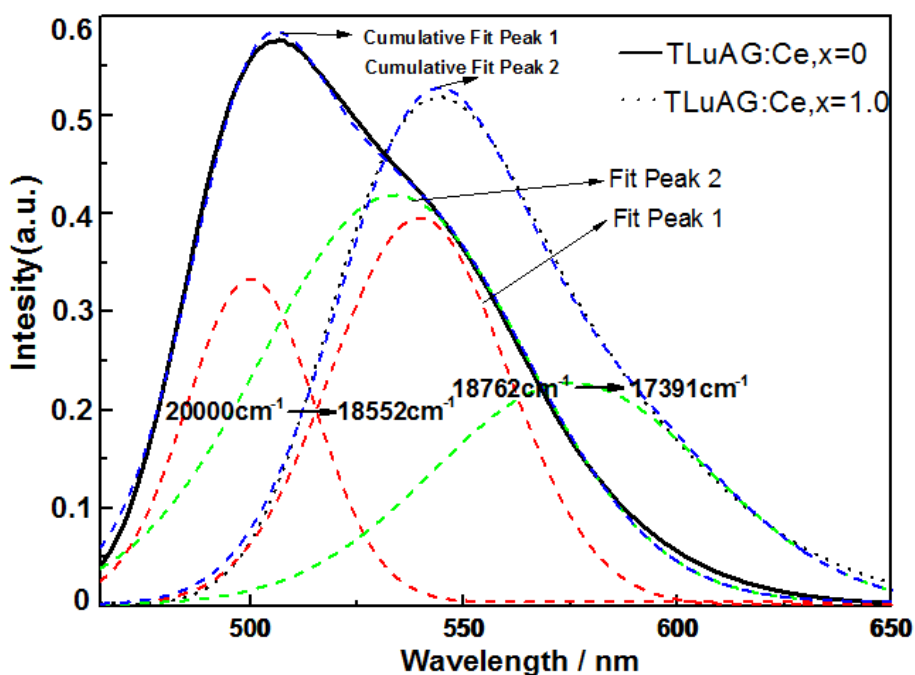


Figure 7. Gaussian curve fittings of $(Tb_xLu_{1-x})_{2.9}Al_5O_{12}: 0.1Ce$ phosphors. $x=0, 1.0$.

The variations in color coordinates (x, y) of $(\text{Tb}_x\text{Lu}_{1-x})_{2.9}\text{Al}_5\text{O}_{12}: 0.1\text{Ce}$ are shown in Fig. 8. Under 450 nm excitation, with the increase of Tb^{3+} in garnet structure, it shifts towards the saturated colors. And, the samples turn green to orange.

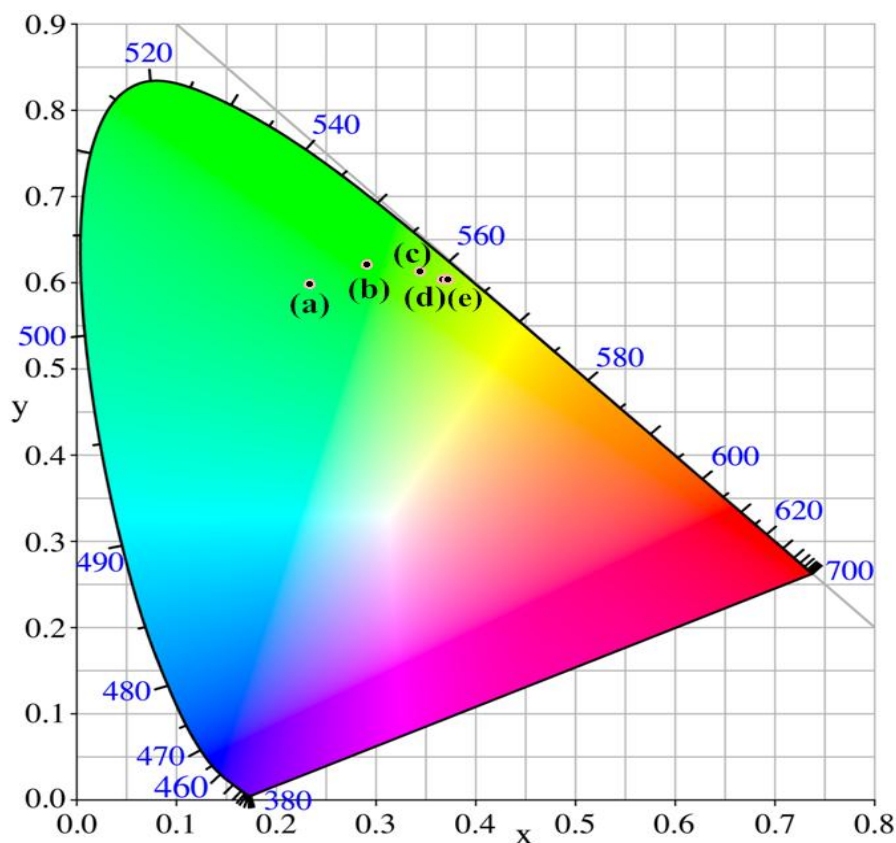


Figure 8. CIE coordinates of $(\text{Tb}_x\text{Lu}_{1-x})_{2.9}\text{Al}_5\text{O}_{12}: 0.1\text{Ce}$ phosphors. a~e: $x=0, 0.2, 0.5, 0.8,$ and 1.0 .

4. CONCLUSIONS

Green to orange tunable Terbium-lutetium aluminum garnet doped with Ce^{3+} ions have been prepared by solid state reaction. With the substitution of Lu^{3+} ion sites by Tb^{3+} ion in garnet structure, XRD patterns show that the LuAG phase changed gradually to the TAG phase, and with the increase of Tb^{3+} , the samples are still cubic structure SEM morphologies indicate that the average particle size of the powders improves. Subjected to the decrease of the difference between the energy centroids of the $5d^1$ and $4f^1$ configurations and the increase of the effective ligand field on the Ce-5d shell associated with electronic effects of Tb^{3+} substituting for Lu^{3+} , the emission band shift toward a longer wavelength by about 37 nm (507 nm to 544 nm) and shift towards the saturated colors, but the emission intensity of the sample continuously decreases. Depending on the mutual doping effects of Lu^{3+} and Tb^{3+} , it exhibits the ability to tune the green to orange phosphors, which benefits to improve the current white LED.

ACKNOWLEDGEMENTS

This work is financially supported by the National Natural Science Foundation of China (No.51302330, 51402032), Natural Science Foundation of Chongqing (No.cstc2012jjA50039), and Science and Technology Project Foundation of Chongqing Education Committee (No.KJ1401102).

References

1. S. Nakamura, T. Mukai and M. Senoh, *Appl. Phys. Lett.*, 64 (1994) 1687
2. Q. Su, H. Wu, Y. Pan, J. Xu, C. Guo, X. Zhang, J. Zhang, J. Wang and M. Zhang, *J. Rare Earths*, 23 (2005) 513
3. X. Piao, T. Horikawa, H. Hanzawa and K. Machida, *Chem. Lett.*, 35 (2006) 334
4. S. H. Chen, J. M. Lin, *Opt. Laser Technol.*, 44 (2012) 169
5. A. Speghini, F. Piccinelli and M. Bettinelli, *Opt. Mater.*, 33 (2011) 247
6. S. A. Hassanzadeh-Tabrizi, *Adv. Powder Technol.*, 23 (2012) 324
7. L. Mancic, K. Marinkovic, B. A. Marinkovic, M. Dramicanin and O. Milosevic, *J. Eur. Ceram. Soc.*, 30 (2010) 577
8. Y. Sang, H. Liu, X. Sun, X. Zhang, H. Qin, Y. Lv, D. Huo, D. Liu, J. Wang and R. Boughton, *J. Alloys Compd.*, 509 (2011) 2407
9. J. M. Ogieglo, A. Zych, T. Jüstel, A. Meijerink and C. R. Ronda, *Opt. Mater.*, 35(3) (2013) 322
10. W. Drozdowski, K. Brylewa, M. E. Witkowski, A. J. Wojtowicz, K. Kamada, T. Yanagida and A. Yoshikawa, *Radiat. Meas.*, 56 (2013) 80
11. L. Wang, M. Yin, C. Guo and W. Zhang, *J. Rare Earths*, 28 (2010) 16
12. T. Y. Choi, Y. H. Song, H. R. Lee, K. Senthil, T. Masaki and D. H. Yoon, *Mat. Sci. Eng. B*, 177 (2012) 500
13. S. H. Lee, H.Y. Koo, D. S. Jung, J. M. Han and Y. C. Kang, *Opt. Mater.*, 31 (2009) 870
14. M. S. Tsai, G. M. Liu and S. L. Chung, *Mater. Res. Bull.*, 43 (2008) 1218
15. L. Kong, S. Gan, G. Hong and J. Zhang, *J. Rare Earths*, 25 (2007) 692
16. Q. Shao, Y. Dong, J. Jiang, C. Liang, J. He, *J. Lumin.*, 131 (2011) 1013
17. V. P. Dotsenko, I. V. Berezovskaya, E. V. Zubar, N. P. Efryushina, N. I. Poletaev, Y. A. Doroshenko, G. B. Stryganyuk and A. S. Voloshinovskii, *J. Alloys Compd.*, 44 (2013) 159
18. A. A. Setlur, J. J. Shiang and C. J. Vess, *J. Phys. Chem. C.*, 115 (2011)3475
19. T. Han, S. Cao, L. Peng, D. Zhu, C. Zhao, M. Tu and J. Zhang, *Opt. Mater.*, 34 (2012) 1618
20. A. B. Muñoz-García, J. L. Pascual, Z. Barandiarán and S. Luis, *Physical Review B.*, 82 (2010) 064114
21. Y. X. Pan, W. Wang, G. K. Liu, S. Skanthakumar, R. A. Rosenberg, X. Z. Guo and K. K. Li, *J. Alloy. Comp.*, 488 (2009) 638
22. T. Y. Tien, E. F. Gibbons, R. G. DeLosh, P. J. Zacmanidis, D. E. Smith and H. L. Stadler, *J. Electrochem. Soc.*, 120 (1973) 278
23. H. S. Jang, W. B. Im, D. C. Lee, D. Y. Jeon and S. S. Kim, *J. Lumin.*, 126 (2007) 371
24. P. D. Rack and P. H. Holloway, *Mat. Sci. Eng. R*, 21 (1998) 171
25. L. Zhang, H. Z. Wang, N. C. Xu, L. X. Wang and Q. T. Zhang, *Chinese Journal of Inorganic Chemistry*, 27(2011)1249
26. J. Z. YU, *Optoelectronic Technology of Semiconductor*. Chemistry Industry Press, Beijing(2003)